IEEE Access
Multidisciplinary ⋮ Rapid Review ⋮ Open Access Journal

Received 16 October 2024, accepted 7 November 2024, date of publication 18 November 2024, date of current version 3 December 2024.

Digital Object Identifier 10.1109/ACCESS.2024.3501577

APPLIED RESEARCH

Investigation of Variable Transformers Using Orthogonal Biasing

JONAS PFEIFFER[1], (Member, IEEE), CAMILO SUAREZ BUITRAGO[2], (Member, IEEE), PIERRE KÜSTER[3], HANS WOUTERS[2], (Graduate Student Member, IEEE), WILMAR MARTINEZ[2], (Senior Member, IEEE), JENS FRIEBE[3], (Senior Member, IEEE), AND MICHAEL SCHMIDHUBER[1]

[1]SUMIDA Components and Modules GmbH, 94130 Obernzell, Germany
[2]Department of Electrical Engineering (ESAT), KU Leuven, 3590 Diepenbeek, Belgium
[3]Department of Electrical Power Engineering, University of Kassel, 34121 Kassel, Germany

Corresponding authors: Jens Friebe (friebe@uni-kassel.de), Wilmar Martinez (wilmar.martinez@kuleuven.be), and Michael Schmidhuber (mschmidhuber@eu.sumida.com)

This work was supported by German Federal Ministry of Economic Affairs and Climate Action (BMWK) under Grant 03EI6104D.

ABSTRACT Magnetic devices are used as passive components in almost all power electronic applications. The use of active premagnetization is one way of designing these components with controllable parameters during operation. As a result, the applications in which these components are used can be further improved. The use of active premagnetization in transformers is of particular interest because they are an integral part of numerous converter topologies in order to ensure the required galvanic isolation or to enable high voltage ratios. In this article, various approaches to variable transformers are presented and discussed. Verification is carried out using 3D FEM simulation and measurements. The focus is on orthogonal biasing as the premagntization method used.

INDEX TERMS Controllable magnetics, magnetic flux interaction, superposition, transformer.

I. INTRODUCTION

Magnetic devices are important components, especially in power electronic applications, where they fulfil various functions. In order to gain an additional degree of freedom in the design and operation of the electrical circuit and thus further improve its parameters, the use of controllable magnetic components is becoming increasingly important. According to [1], variable inductors are widely used, e.g., in applications for light drivers.

Variable transformers, on the other hand, are rarely the subject of investigations. A few examples are shown in [1]. Furthermore, several approaches are investigated in [2], [3], [4], [5], and [6], in which various methods of active premagnetization are used.

These variable transformers can support the operation of a topology. Especially in resonant circuits, e.g., a LLC converter, they are a promising approach to provide the required variation range. Two examples are shown in [7].

This technology approach can also be used to further improve the Dual Active Brigde (DAB), especially regarding loss reduction and soft switching. A detailed analysis of several design approaches of variable transformers for DAB converters is presented in [8]. A promising improvement in combination with a proper control scheme was published in [9].

Considering the mentioned design approaches for variable transformers, orthogonal biasing is rarely used. Thus, the following patent of a transformer with orthogonal biasing exists [10].

A long-used principle based on a transformer with orthogonal biasing is the so-called ''parametric transformer'' or ''paraformer''. This consists of two wound C cores that are rotated by 90° to each other. The resulting magnetic flux curves can be counted as orthogonal biasing. The principle of the paraformer is presented in detail in [11]. However, it is only suitable for transmitting high power to a limited extent.

The associate editor coordinating the review of this manuscript and approving it for publication was Chunhua Liu.

The use of orthogonal biasing can be advantageous compared to the other premagnetization methods. In particular, if strong feedback to the auxiliary winding is to be expected, this can be greatly reduced by decoupling the main and auxiliary flux due to their orthogonal arrangement.

For this reason, different variants of variable transformers using orthogonal biasing are presented in this article. The approaches shown are intended for use in DC-DC converters. The first design enables an adjustable effective turns ratio, which is particularly useful for Dual Active Bridge (DAB) topologies. The second approach modifies the leakage inductance in particular, while the main inductance remains almost the same. This approach is particularly suitable for resonant converter topologies. Of course, other areas of application beyond these topologies are conceivable and feasible.

After a brief overview of the effect of orthogonal biasing in Section II, the manufacture of the required drill holes in the ferrite material is outlined in Section III.

Subsequently, general investigations on the impact of this premagnetization method on ferrite cores are presented in Section IV. These are extended by specific investigations into the saturation characteristics of the core material around the drill holes in Section V. These are incorporated into the development of an improved design.

Two different approaches for variable transformers are presented within the following two sections. While the first approach in Section VI pursues an adjustable effective turns ratio, the second approach in Section VII affects the leakage inductance of the magnetic component.

The investigated variable inductors and transformers are compared regarding their variation range in Section VIII. Finally, the presented approaches are discussed in Section IX. A critical reflection of the investigated magnetic components is carried out. From this, open research questions and approaches for further development can be derived.

II. THEORETICAL PRINCIPLES OF ORTHOGONAL BIASING

Premagnetization of either the entire magnetic core or individual sections can be implemented as an active or passive design. Passive premagnetization is achieved by using permanent magnets, which are introduced within or along the path of the magnetic flux. The permanent magnet generates an additional auxiliary magnetic flux, which is parallel to the main magnetic flux of the winding. Their directions are either the same or opposite. Detailed investigations of passive premagnetization in inductors for power electronic converters are presented and discussed in [12].

For the usage of active premagnetization, an auxiliary winding instead of a permanent magnet is implemented. The winding is wound on or introduced in the magnetic core. If a current flows through the auxiliary winding, an auxiliary flux is generated within the core material. According to [13], active premagnetization can be achieved by the following three different methods:

- parallel biasing
- mixed biasing
- orthogonal biasing

The differences between these methods, their implementation on or within the magnetic core material, as well as their mode of action and the associated impacts on the magnetic core, are presented and discussed in detail in [14] and [15].

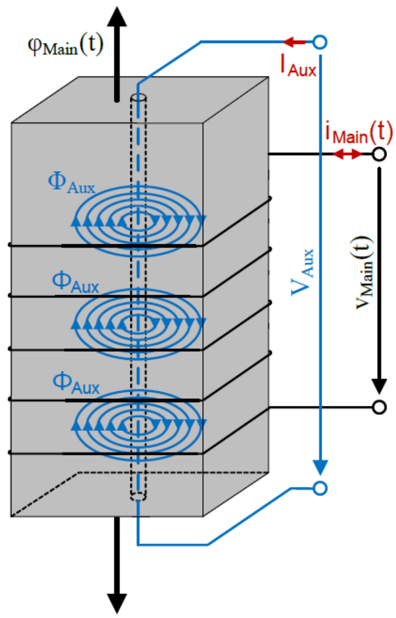

FIGURE 1. The principle of orthogonal biasing: An auxiliary DC winding is introduced into the core section through drill holes. The auxiliary magnetic flux is orthogonal to the main flux. [13].

The principle of orthogonal biasing is shown in Fig. 1. One or more holes are manufactured into a magnetic core section. An auxiliary winding is introduced in these holes. The auxiliary magnetic flux generated by the current through the auxiliary winding is orthogonally aligned to the magnetic main flux of the main winding. According to the theory of superposition, the coupling between both windings should be zero. As a result, the magnetic fields, as well as the magnetic fluxes of main and auxiliary winding, theoretically should not affect each other. Practical investigations, on the other hand, show a mutual impact of the windings. This observation can be explained by nonlinearities of the core material. Furthermore, almost all standard core geometries have sections where main and auxiliary magnetic fluxes are not orthogonally aligned. If, e.g., an EE-core is orthogonally biased within its center leg, main and auxiliary magnetic fluxes will not be orthogonally aligned in the section where the center leg transitions into the yoke as it is shown in Fig. 2.

If a current flows through the auxiliary winding, an auxiliary magnetic flux is generated, which affects the area around the auxiliary winding. By increasing the current, the core material around the auxiliary winding saturates. The saturation spreads in the direction of the outer edges of the core section by further increasing the current. Thus, the cross-sectional area in this section available to the magnetic

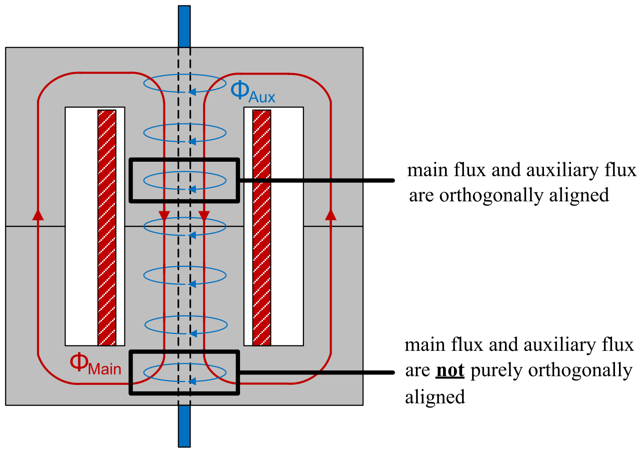

FIGURE 2. An EE core with orthogonal biasing within the center leg. Magnetic main flux (red) and auxiliary flux (blue) are orthogonally aligned within the middle of the center leg. Both magnetic fluxes are not purely orthogonally aligned within the transition section from the center leg to the yoke. [16].

main flux is reduced. As a result, the hysteresis loop, as well as the magnetization curve, is sheared as depicted in Fig. 3. The inductance value of the magnetic device decreases.

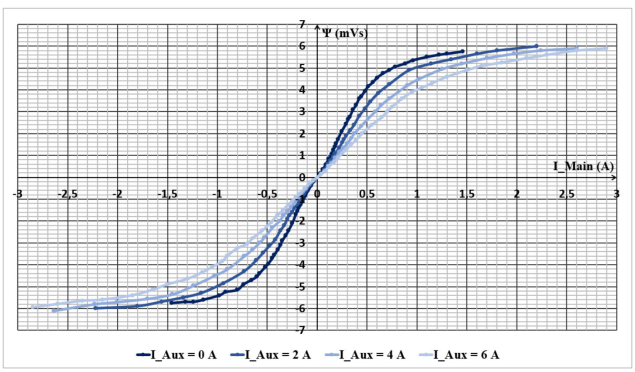

FIGURE 3. Magnetization curve at orthogonal biasing: The original curve (dark blue) is sheared (light blue) by increasing the auxiliary current. [14], [15].

If more than one hole is used, the direction of the current through every hole is important. The usual realization is an arrangement of opposite-aligned current directions of neighbouring holes. For example, consider four holes arranged in a square; the direction of a current results in a crosswise arrangement. However, other current direction arrangements that deviate from the standard may be more effective in certain situations, according to [15] and [17].

Due to the challenges of the manufacturing process regarding the holes within the core material (see Sec. III), it has to be checked if this biasing method is suitable for the used core material. Especially if anisotropic materials are used, as well as materials where a high magnetic field strength is needed to reach the saturation flux density, e.g. iron powder.

The usage of orthogonal biasing in laminated cores, e.g., laminated iron cores, is not recommended. The biasing method will have only a very weak to no impact on the magnetic core because of the small air gaps between the individual core sheets.

III. MANUFACTURING PROCESS OF HOLES IN MAGNETIC CORE MATERIALS

As mentioned in Section II, manufacturing holes into a core material can be challenging, especially if a ceramic material like ferrite is used. Ferrite materials are very brittle and fragile. Manufacturing or machining the core material can cause damage to it. A possible approach to avoid subsequent machining is to use core geometries that already have holes as standard, such as P-cores, PM-cores, some UR-cores, etc. when designing the magnetic component. The mentioned core geometries are well suited for orthogonal biasing because of their circular (center) leg.

If a manufacturing process is inevitable, an Ultrasonic/Sonic Driller/Corer (USDC) can be used. This process is very cost-intensive and, therefore, is only suitable for small quantities. However, attention has to be be paid to the manufacturing limits of the respective USDC with regard to hole diameter and drilling depth in order to avoid damaging the drilling tool. If larger quantities are needed, the fabrication of a press die might be more economical. This means that the ferrite cores are already produced with the required holes so that there is no need for post-processing by USDC is no longer necessary.

If iron powder cores are to be drilled, the problem of subsequent machining will be exacerbated because the material is considerably more brittle than ferrite. However, analogous to ferrite cores, the insertion of the holes by a press die can be integrated directly into the regular production process for large quantities.

In the case of cores made from laminated iron sheet packs, less attention has to be paid to mechanical damage to the material than to preserving its magnetic properties. The sheets used are usually provided with a magnetic orientation by rolling and annealing. This can be sensitive to mechanical or thermal stress. For small quantities, the required individual sheets are usually manufactured by laser cutting. This means that the holes can be cut out during the production process. during the production process. Laser cutting is a cost-effective cutting process that requires only minimal post-processing. In addition, this process allows any core geometries and hole arrangements to be produced very precisely. precise production. For high volumes, a punching tool may prove more economical than laser cutting. As already mentioned in Section II, orthogonal biasing is not suitable for laminated cores in almost all use cases.

IV. GENERAL INVESTIGATIONS

According to Section III, manufacturing holes into a magnetic core material can be a challenging and cost-intensive process. For this reason, the number of holes required to achieve the desired effect should already be taken into account during the design of the component. A simple modelling approach for the number and arrangement of holes based on circle packaging is presented in [16].

Furthermore, when using active premagnetization of magnetic components, an air gap inserted in the component has to be taken into account because it significantly weakens the influence of premagnetization on the change of the inductance value.

To show the impact of the air gap on the adjustability of the inductance value, an EE 80/38/20 and a URR 70/50/22 were studied. Originally, a URR 70/65/22 should have been used, but its legs had to be shortened due to the maximum drilling depth of the Ultrasonic/Sonic Driller/Corer (USDC) tool. Both cores are made of the ferrite material Fi324 from the manufacturer SUMIDA. While a single hole was drilled in the center of the central leg of the EE 80/38/20 core, both legs of the URR 70/50/22 core were drilled with a hole in the center. They are shown in Fig. 4.

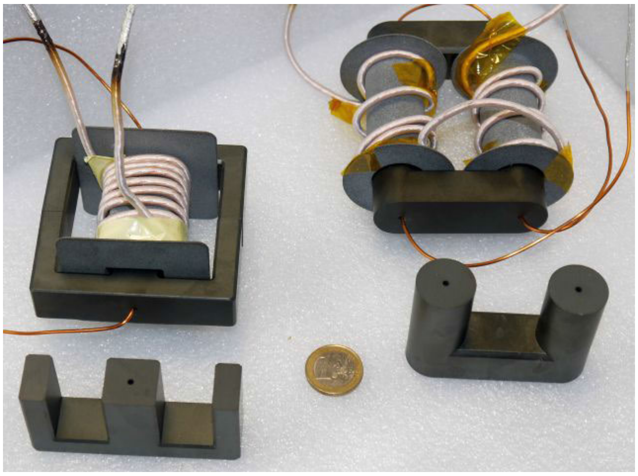

FIGURE 4. Investigated premagnetized cores (EE 80/38/20 and URR 70/50/22).

The results of the EE 80/38/20 core are shown in Fig. 5, while those of the URR 70/50/22 core are shown in Fig. 6. The air gap length given in the diagrams refers to the total air gap length.

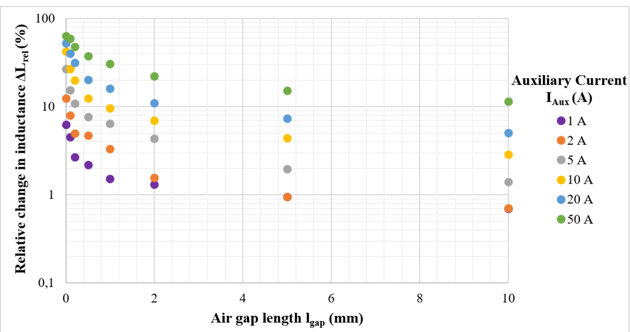

FIGURE 5. Impact of the air gap on the relative change of the inductance of the EE 80/38/20 core.

Both figures show that the variable inductance range decreases with increasing air gap length. This effect can be partially compensated by increasing the auxiliary current.

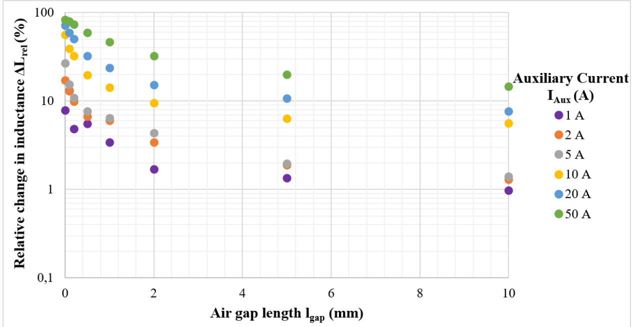

FIGURE 6. Impact of the air gap on the relative change of the inductance of the URR 70/50/22 core.

Furthermore, it can be seen that with these used cores, significant changes in inductance ($\Delta L_{rel} \geq 10\,\%$) are only possible with very large auxiliary currents ($I_{Aux} \geq 10\,\text{A}$) from an air gap length of $l_{gap} = 2\,\text{mm}$.

Due to the circular leg cross-section, the URR core can be better controlled than the EE core, where the corners of the square cross-section are only partially saturated by the circular lines of the auxiliary magnetic flux of the orthogonal biasing. This phenomenon is already addressed and explained in more detail in [16]. Due to the better modulation of the URR core, larger changes in the inductance value are possible with the same auxiliary current.

V. NON UNIFORM CROSS SECTIONAL AREA

In this section, the effect of non-uniform cross-sectional areas on the orthogonal biasing of cores is investigated through two commercially available core types. A comprehensive analysis is carried out to reveal the limitations and complications of orthogonal biasing implementation based on both small and large signal simulations and experimental validation.

Fig. 7a illustrates a pot core designed to house internal windings. This configuration closely resembles the ideal orthogonal magnetization design discussed in [18], with the inclusion of two opposing holes to facilitate the insertion of internal windings. However, as depicted in Fig. 7b, this minor difference results in local saturation by reducing the cross-sectional area for the flux excited by the external winding. In this arrangement, the internal winding serves as the primary winding, while the external winding functions as the control winding, as indicated in Fig. 7c.

Note that a winding swap leads to a similar situation, where the flux density in the inner section of the core is larger than in the external part because of differences in the internal and external core radii and ultimately the transversal areas. Furthermore, in the selected winding configuration, the capacity of the control winding to accommodate a large number of turns enables a reduction in the biasing current and the associated copper losses. However, regardless of the winding arrangement, it is shown that even small deviations from the ideal core shape can significantly impact the achievement of an even saturation profile.

(a) External control winding

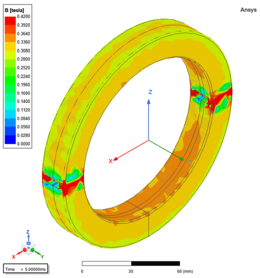

(b) Control flux density

(c) Internal main winding

FIGURE 7. **P 148/112/10 core based variable inductor [19].**

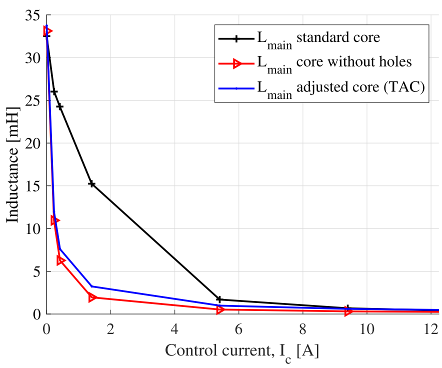

(a) Simulations of the main inductance as function of the control current for the standard core, the core without holes and the proposed adjusted core

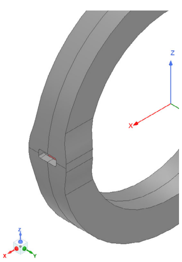

(b) Proposed core area adjustment (TAC)

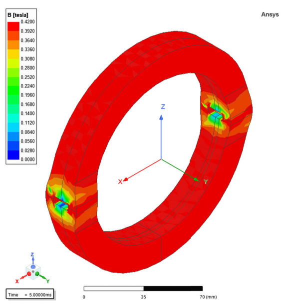

(c) Saturation profile of the adjusted core

FIGURE 8. **Proposed (TAC) modification on the P 148 core: simulations and comparison with the standard core [19].**

Simulations of the core geometry under small-signal conditions were conducted using FEA to analyse its characteristics. Fig. 8a displays the main inductance as a function of the control current, demonstrating its behaviour as a variable inductance. When compared to the same core structure without holes, as shown in the same figure, it is clear that a lower current is needed to achieve the same inductance levels when a uniform cross-sectional area is ensured.

The magnetic field distribution in Fig. 7b shows that there are considerable inhomogeneities near the holes. The high flux density in this reduced area leads to saturation of the core, which increases the local reluctance and reduces the control flux, leaving the rest of the core unsaturated. This results in a limited achievable change of inductance, which is in agreement with the constraints for orthogonal biasing identified in [14]. To further investigate this issue and confirm that it is caused by the non-uniform cross-sectional areas, an adjusted FEM model was created featuring additional ferrite material surrounding the holes, as seen in Fig. 8b-8c. This TAC modification largely compensates for the area reduction caused by the holes. As demonstrated in Fig. 8a, this adjustment successfully prevents local saturation, resulting in a significant improvement in the homogeneity of the magnetic field.

(a) Modified core cross-sectional area by adding ferrite blocks at high flux density zones

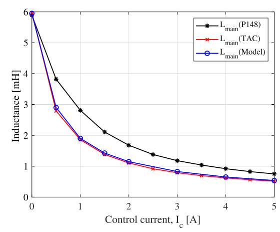

(b) Small-signal characterisation

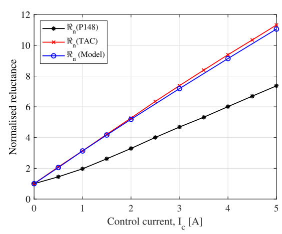

(c) Normalised core reluctance variation

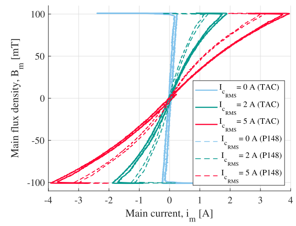

(d) Flux density curve as a function of the main current (large-signal characterisation)

FIGURE 9. **Experimental results modified core vs. model.**

The experimental results, as shown in Fig. 9, are consistent with the behaviour expected from the simulations. Although there are variations in the inductance values, these can be attributed to the considerable uncertainty in the air gap size that is inherent in the experimental setup and the TAC implementation technique, where ferrite blocks were placed near the core openings.

The experimental validation of the results at the small-signal level was carried out using a current source supply (Voltec DC1000) in series with the control winding, while the main inductance was measured using a Wayne Kerr Magnetics Analyser 3260B. For large-signal experimental measurements, the main winding was excited using a full-bridge inverter, generating a square-wave voltage of 130 V at 20 kHz. Thus, the maximum flux density in the main winding is maintained at a constant of 100 mT. The parameters of the inductor can be found in Table 1.

TABLE 1. P 148/112/10 core based variable inductor core prototype parameters.

Parameter	Value
Number of turns of the main winding (N_m)	10
Number of turns of the control winding (N_c)	245
Core reference	P 148/112/10
Material	BFM8
Main effective path length (l_{e_m})	48 mm
Main effective area (A_{e_m})	1457 mm^2
Control effective path length (l_{e_c})	408 mm
BFM8 ferrite block dimensions	20 mm x 10 mm x 10 mm

As observed, with the addition of material at sections with a smaller transversal area on the control flux path, the reluctance variation increases by 54 % compared to the standard core. Despite the fact that the implemented core modification lacks a smooth cross-sectional profile, it proves to be effective. Additionally, the proposed correction to the core closely matches the expected theoretical core performance without the holes (see Fig. 9b), primarily because the altered zone is relatively small for the main flux path, rendering it negligible. In fact, the main inductance without the ferrite blocks is 5.89 mH, whereas with the addition of four of them, it is 5.97 mH.

Furthermore, considering the inductor large signal characterization presented in Fig. 9d, it is evident that the transversal area compensation technique (TAC) does not, in this case, lead to any alteration of the expected B-H curves. The figure illustrates a substantial linear region for various control currents, characteristic of orthogonal biasing.

Pot and UR cores are commonly used for orthogonal biasing due to their built-in holes, which facilitate the implementation of the auxiliary windings. However, non-uniform cross-sectional areas in these structures result in uneven control flux distribution, thereby limiting the variation in the core reluctance. For instance, in the URR 64/40/20-3C90 core illustrated in Fig. 10a, the outer area A_1 is smaller than the inner area A_2, leading to a higher control flux density at the core sides compared to the center. This uneven distribution can be observed in the FEA simulation of Fig. 10b, where an auxiliary or control current $I_c = 8A$ is applied.

Consequently, regions of low control flux density (depicted in yellow) create a low reluctance path for the main flux circulation, thereby diminishing the impact of the control winding.

Based on this observation, improving the uniformity of the auxiliary flux density can be achieved by slightly reducing the inner core area ($A_3 < A_2$), as depicted in Fig. 11a. This modification leads to a higher saturation in the inner region of the core, as demonstrated in the simulation results of Fig. 11b, where the same auxiliary or control current ($I_c = 8A$) is employed. When the inner core area is reduced, the aforementioned low reluctance path is eliminated, resulting in a higher drop in the main inductance for the same control current I_c.

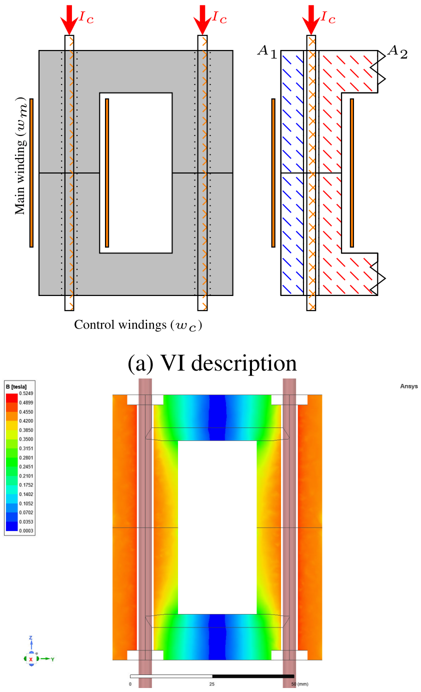

(a) VI description

(b) Saturation profile

FIGURE 10. VI description and saturation profile (off-the-shelf core).

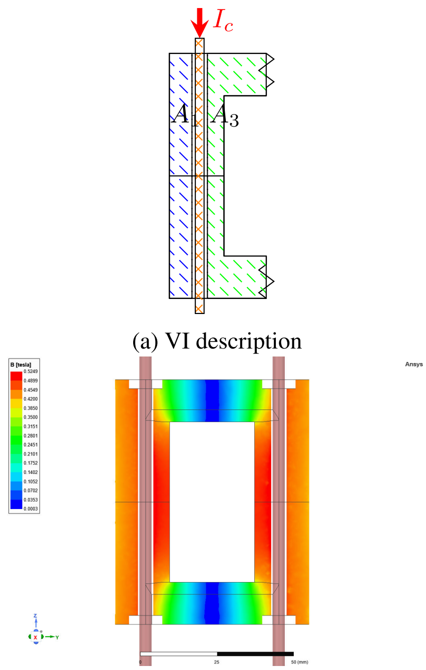

(a) VI description

(b) Saturation profile modified core

FIGURE 11. VI description and saturation profile (modified core).

(a) off-the-shelf core

(b) Modified core

FIGURE 12. **UR core comparison.**

To experimentally verify this concept, the inner sides of the core limbs were ground by 2 mm, as shown in Fig. 12. Using the previously described setup, the main inductance of the variable inductor was characterized at the small-signal level, following the parameters presented in Table 2.

TABLE 2. **UR core VI prototype parameters small-signal characterisation.**

Parameter	Value
Number of turns of the main winding (N_m)	13
Number of turns of the control winding (N_c)	3
Characterisation frequency	100 kHz
Characterisation voltage	1 V

Fig. 13 displays the device under test, the setup, and the small-signal characterization results. As observed, a significant improvement in the core saturation profile is achieved, resulting in an inductance four times lower than when using the off-the-shelf core. Although the proposed modification reduces the transversal area of the main flux path, its impact on the main inductance for $I_c = 0$ A is minimal, with values of 749 μH and 721 μH obtained for the original and modified cores, respectively.

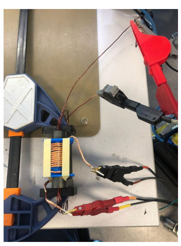

(a) Device under test

(b) Measuring setup

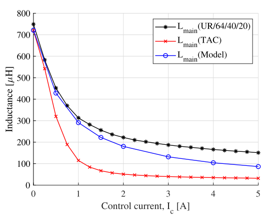

(c) Inductance variation

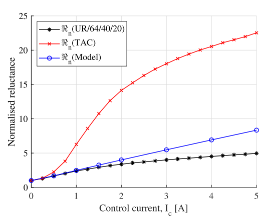

(d) Normalized reluctance variation

FIGURE 13. **Small-signal characterization comparison: setup and results.**

Despite the significant reduction in material permeability at lower control current levels indicated by the small-signal characterization results, further confirmation is required at the large-signal level. To achieve this, a high-frequency inverter is employed to excite the main winding of the inductor, while the auxiliary winding is connected in series with an air-core inductor and a voltage source, maintaining a quasi-constant control current, as illustrated in Fig. 14a. In the experimental setup depicted in Fig. 14b, the inverter TDINV3500P100 operates at a switching frequency of 25 kHz, generating square voltage wave-forms with amplitudes up to 500 V. These voltage levels correspond to a maximum main magnetic flux density (B_m) of approximately 300 mT, as defined by equation (1).

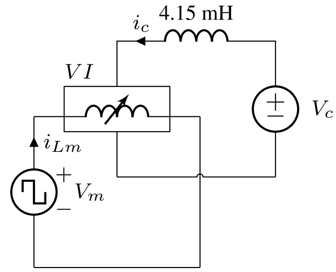

(a) Characterization circuit

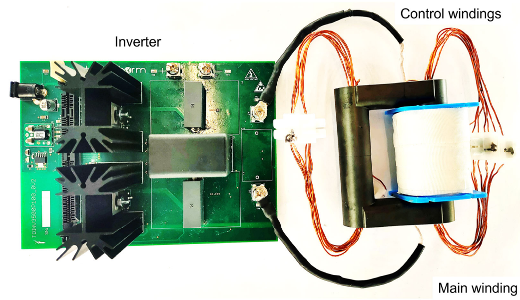

(b) High-frequency inverter and device under test

FIGURE 14. **Large-signal characterization setup.**

$$B_m = \frac{V_m}{4 f_s N_m A_{e_m}} \tag{1}$$

where: V_m: Main voltage amplitude
f_s: Main voltage waveform frequency
A_{e_m}: Equivalent main-path core area

Table 3 provides the specifications of the tested inductor and the modified core.

TABLE 3. **VI prototype parameters - Large-signal characterization.**

Parameter	Value
Number of turns of the main winding (N_m)	52
Number of turns of the control winding (N_c)	8
Main effective core area (A_{e_m}) in mm^2	279
Main effective core length (l_{e_m}) in mm	210

The B-H curve associated with the variable inductor is illustrated in Fig. 15. As seen, the material's permeability undergoes a significant decrease when exposed to magnetic flux densities below 50 mT, as indicated by the bold lines. Furthermore, the curve maintains its linearity, which is

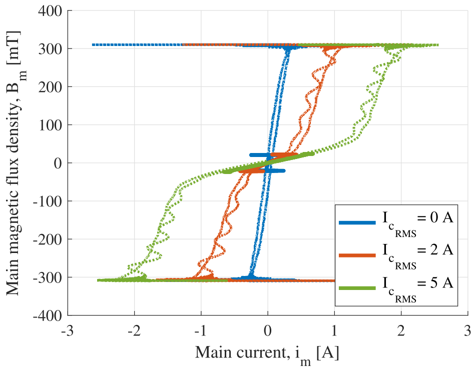

FIGURE 15. **Modified core B-H curves: Large (dotted lines) and small (bold lines) signal comparison.**

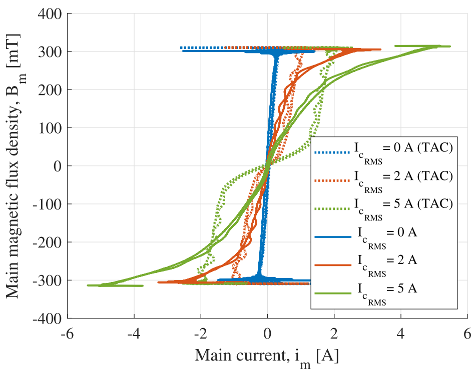

FIGURE 16. **B-H curve comparison between the VI with the modified core (dotted lines) and the off-the-shelf core (bold lines).**

commonly observed as a result of orthogonal biasing of the core. However, in the case of higher magnetic flux densities, the B-H curve displays a distinctive double ''S'' shape, indicating the presence of mixed or parallel biasing and implying a heightened interaction between the main and control magnetic fluxes.

To investigate whether the alteration of the magnetic core is accountable for this behavior, an inductor with the identical turns configuration but utilizing an off-the-shelf core was characterized and compared to the previous results, as depicted in Fig. 16. The comparison reveals that the modification indeed impacts the interaction of the fluxes, particularly noticeable at higher flux densities.

Fig. 17 shows the relationship between changes in the inductor current and variations in device inductance relative to the auxiliary current. These variations occur for magnetic core flux densities within and outside the linear region of the B-H curve. Specifically, for $V_m = 30$ V, the inductor current (i_{Lm}) maintains a constant slope independent of the main voltage amplitude (V_m), as shown in Fig. 17a. However, as the main voltage increases and the magnetic flux density (B_m) exceeds 50 mT, the inductor currents exhibit varying slopes, indicating nonlinear behavior (Fig. 17b). These findings align with the observations presented in Fig. 15. Furthermore, under these conditions, the control current (i_c) demonstrates oscillations, highlighting the influence of the main flux on the control winding.

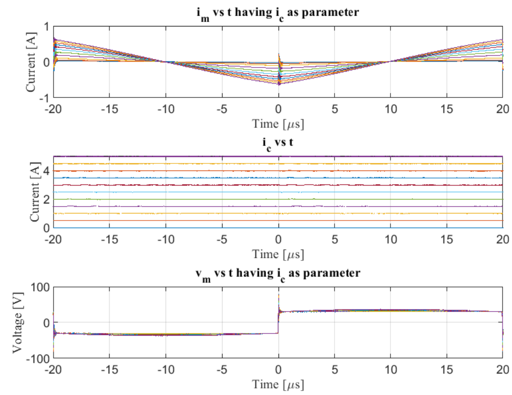

(a) $V_m = 30$ V

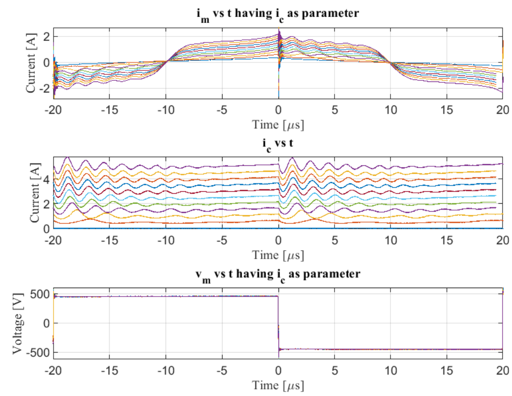

(b) $V_m = 450$ V

FIGURE 17. **VI (modified core) current and voltage wave-forms having i_c as parameter varying form 0 A to 5 A with 0.5 A steps.**

In comparison, Fig. 18 illustrates the waveforms of the inductor currents for the variable inductor using the off-the-shelf core. While these currents are not linear, their shape is closer to the expected behavior of a variable inductor controlled through orthogonal biasing.

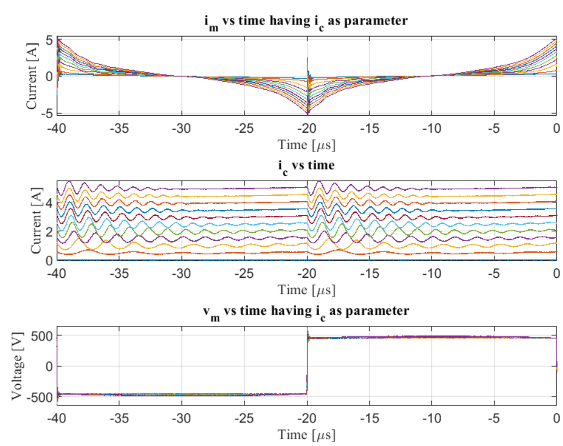

FIGURE 18. **VI (off-the-shelf core) current and voltage wave-forms having i_c as parameter varying form 0 A to 5 A with 0.5 A steps.**

This section highlights the significant impact of non-uniform cross-sectional areas in the core on the maximum variation of reluctance in controllable devices using orthogonal biasing. The modification of this condition through the addition or removal of magnetic material in the core can result in a closer approximation to the ideal interaction among orthogonal fields, resembling the behavior of ideal core shapes such as hollow toroids or cylinders. While this technique leads to substantial improvements, it should be noted that its benefits may be limited to restricted variations in the main magnetic flux densities. Therefore, careful consideration of the core shape and its suitability to the specific application is necessary to fully leverage this feature's advantages.

VI. VARIABLE TRANSFORMER

The utilization of the UR core structure (modified core), in conjunction with the integration of the orthogonal biasing technique discussed in Section V, can be extended to facilitate the implementation of a controllable/variable transformer (VT), as depicted in Fig. 19. By incorporating these advancements, the coupling factor between the primary winding (having n_p turns) and the secondary winding (formed by a series connection of windings a and b with n_{s1} and n_{s2} turns, respectively) becomes dependent on the controllable reluctance of the core-set #2, denoted as $\Re_v$.

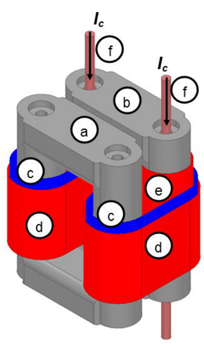

Part	Description
a	UR Core-set #1 ($\Re_1$)
b	UR Core-set #2 ($\Re_v$)
c	Primary winding (w_p having N_p turns)
d	Secondary winding a (w_{s1} having N_{s_1} turns)
e	Secondary winding b (w_{s2} having N_{s_2} turns)
f	Control winding ($w_{c1,2}$ having N_c turns)

FIGURE 19. Orthogonal-bias based VT description [21].

Within this system, the primary winding w_p and the winding w_{s1} are tightly coupled, while the coupling factor with the winding b is subject to the impact of the auxiliary or control current i_c. The ability to modify the core reluctance is achieved through the saturation of core limbs, utilizing the bias flux generated through the auxiliary winding. Consequently, this enables variations in the transformer's effective turns ratio (n_{eq}), as well as the series and the equivalent parallel inductances (l_a and l_b, respectively).

To obtain a thorough comprehension of the transformer's operation, it is necessary to examine its magnetic and

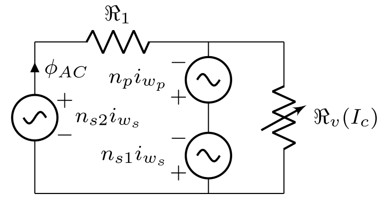

(a) VT magnetic circuit representation

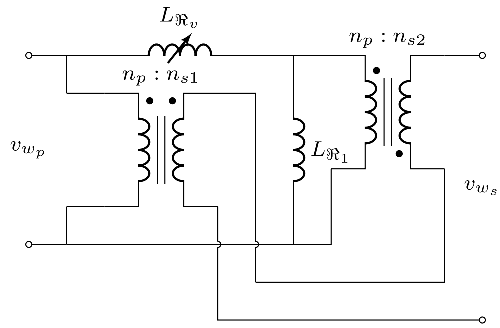

(b) VT electric circuit representation

FIGURE 20. VT small-signal magnetic and electric circuit representation.

electric circuit representations, as displayed in Fig. 20. These visualizations highlight how the control of the leakage flux among the transformer's windings is determined by the current-dependent reluctance $\Re_v(i_c)$, which in turn governs the value of the leakage inductor $L_{\Re_v}$. This parameter has a direct impact on the power transfer between the primary winding and the secondary winding b, which is represented by the ideal transformer characterized by a voltage ratio of $n_p : n_{s2}$.

A straightforward representation of the VT is shown in Fig. 21. The parameters of the cantilever model can be determined by quadripole analysis of the circuit in Fig. 20b. Likewise, for small-signal characterization of a VT prototype, open-circuit and short-circuit tests can be conducted.

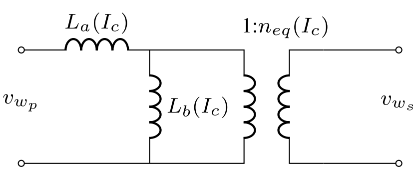

FIGURE 21. VT electrical circuit - cantilever model.

Accordingly, the VT prototype shown in Fig. 22a with its main parameters outlined in Table 4, undergoes characterization, and the corresponding results are depicted in Fig. 22b. For this procedure, the BK precision 891 LCR meter was used at a measurement frequency of 20 kHz.

TABLE 4. Orthogonal bias-based VT prototype parameters.

Parameter	Value
Number of turns of the primary winding N_p	7
Number of turns of the secondary winding N_{s1}	15
Number of turns of the secondary winding N_{s2}	10
Number of turns of the control winding N_c	8

(a) Variable transformer prototype

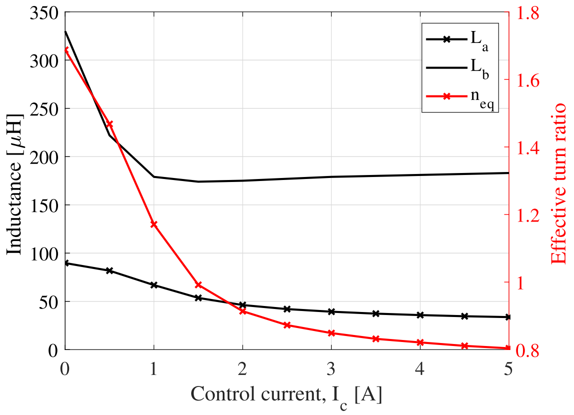

(b) VT cantilever parameters

FIGURE 22. **Variable transformer small-signal characterization.**

As auxiliary or control current I_c rise so does the reluctance $\Re_v$. Consequently, the coupling factor between the windings increases and the effective turn ratio n_{eq} approaches its minimum theoretical value $(n_{s1} - n_{s2})/(n_p)$, which is limited by the stray reluctance of the structure.

Under ideal conditions, $\Re_v|_{I_c=0} \ll \Re_1$ having as a result $n_{eq}|_{I_c=0} \approx n_{s1}/(n_p)$. However, due to the close proximity of the reluctances $\Re_1$ and $\Re_v|_{I_c=0}$, the maximum achievable value of n_{eq} is reduced. For a detailed description and analysis and characterization procedure of a similar transformer analysis using parallel biasing, refer to [20].

VII. TRANSFORMER WITH VARIABLE LEAKAGE INDUCTANCE

The following section discusses the possibilities for controllable leakage inductances for transformers with ferrite core material. A distinction has to be made between tight coupling and loose coupling of the primary and secondary windings. The latter represents a strong yoke leakage and can be used primarily as a model if the two windings are not applied to the same leg (Fig. 23a). Close coupling of the windings is achieved if the two windings are applied to one leg of the core (Fig. 23b). This structure generally achieves very good coupling and therefore very low leakage inductance.

A current-controllable leakage inductance can be realized by additional ferrite sections in the leakage path. The magnetic field for controlling the core section can be

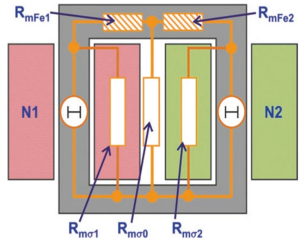

(a) Strong yoke scattering

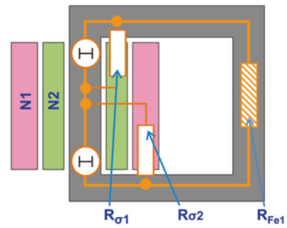

(b) Tight coupling

FIGURE 23. **Modeling of the scattering [22].**

generated by one of the three premagetization methods (parallel, mixed and orthogonal biasing). However, parallel biasing at this point would also impact the core for coupling the primary and secondary windings due to the stray field. In addition, a high level of feedback on the control circuit is to be expected. Mixed or orthogonal biasing is therefore the preferred variant. The focus here should primarily be on orthogonal biasing. As described above, the magnetic circuit to be controlled has to be very well connected to the main path of the magnetic flux in order to achieve the best possible control effect. In the case of strong yoke scattering, however, this also has a significant impact on the coupling core. For this reason, the following case for a close coupling is examined first (see Fig. 24).

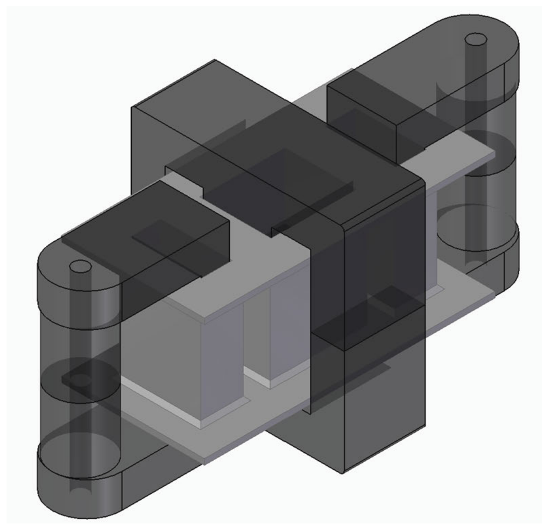

FIGURE 24. **Graphic of the DUT.**

The structure consists of two E cores (EE 55/28/21) for coupling the primary and secondary windings and four UR cores (UR 37/26/18) for the two leakage inductances of the two windings. A hole with a diameter of $d_{hole} = 4\,\text{mm}$ is drilled orthogonally in the round leg of each of the UR cores.

The windings are applied in such a way that the primary winding ($N_1 = 10$) and the secondary winding ($N_2 = 10$) each enclose only one stray core, but together enclose the center leg of the E core. A wire is passed through the hole in each of the UR cores. This symmetrical structure simplifies the equivalent circuit, as the leakage and

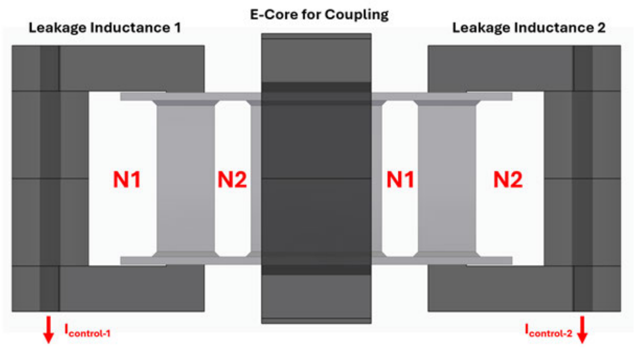

FIGURE 25. Winding arrangement of the DUT.

magnetizing inductance of the primary and secondary sides are approximately identical (see Fig. 26).

The measurements are carried out with the Wayne Kerr 6500 B impedance meter and are therefore small-signal measurements with the transformer open-circuit and short-circuit. A sinusoidal voltage of $V_{source,rms} = 1\,\mathrm{V}$ at $f_{source} = 10\,\mathrm{kHz}$ is selected as the level. In addition, the current in the primary winding is increased in 200 steps from $I_{bias,min} = 0\,\mathrm{A}$ to $I_{bias,max} = 10\,\mathrm{A}$ via a bias unit. The final result is a set of curves due to the variably selectable control current $I_{Control}$, which is selected in 11 steps from $I_{Control,min} = 0\,\mathrm{A}$ to $I_{Control,max} = 10\,\mathrm{A}$, resulting in 11 measurement ranges. In measurement 1, the inductance of the arrangement is measured at the primary winding N_1, whereby the terminals at N2 are open. The bias current flows accordingly through the winding N_1. Eleven characteristic curves are generated by varying the control current $I_{control-1}$ through the leakage inductance 1.

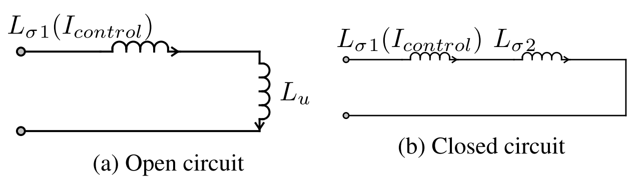

FIGURE 26. Equivalent circuits of open and closed circuit measurements.

In combination with the short circuit measurements (short circuit at N2), the magnetizing inductance and the leakage inductance can be determined using the following formulas.

$$L_{\sigma 2} = \frac{L_{cc}(@I_{control})}{2} \tag{2}$$

$$L_{\sigma 1} = L_{cc}(@I_{control}) - L_{\sigma 2} \tag{3}$$

$$L_{\mu} = L_{oc}(@I_{control}) - L_{\sigma 1} \tag{4}$$

The measurement results show that the magnetization inductance of the arrangement is not affected due to the separate core for the leakage inductance. The small differences are due to measurement uncertainties.

The measurements of the leakage inductances, on the other hand, show a clear effect of the orthogonal biasing. The inductance of the arrangement can be reduced by up to 50 % in the first areas, but can also be increased by up to 90 % in

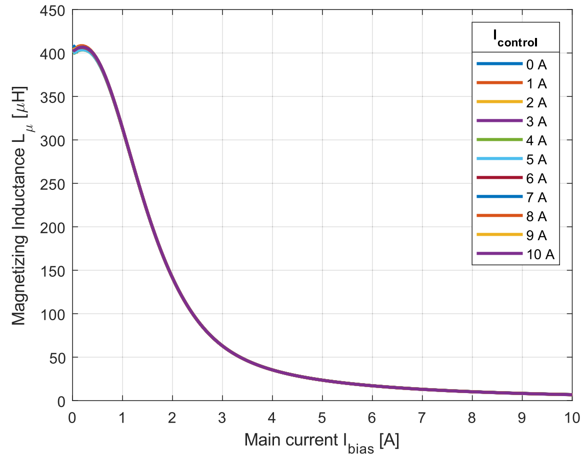

FIGURE 27. Measured magnetizing inductance.

the area of the saturation bend (see Fig. 29). The percentage change is described by the following formula:

$$\Delta L[\%] = \frac{L(@I_{control})}{L(I_{control} = 0A)} \tag{5}$$

In order to record the effect of the premagnetization only on the stray core (UR core), the E core and the second UR core are removed in a further measurement.

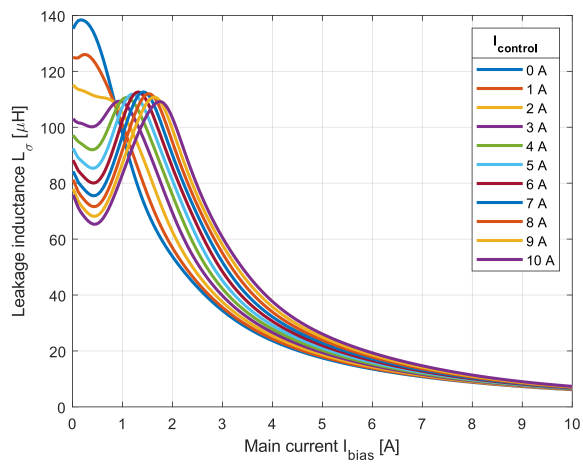

FIGURE 28. Measured leakage inductance.

The impact of the premagnetization can now be clearly seen. While the decrease in inductance is to be expected due to an increasing current, the increase in inductance for the orthogonal biasing is a special feature.

This can be explained by the saturation of the circular leg of the UR core at a magnetic field strength of over $H = 100\,\mathrm{A/m}$. The magnetic field strength can be described by Ampère's law and the results can be compared with the data sheet of the UR core.

$$H_{control} = \frac{I_{control}}{2\pi\, r_{UR\ core}} \tag{6}$$

Field strengths above this lead to a mixed biasing in the yoke of the core, which causes the inductance values to increase. When measuring the leakage inductances using the

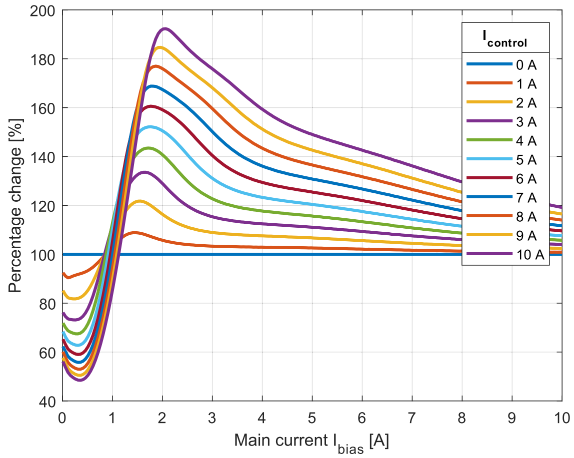

FIGURE 29. Percentage change of the leakage inductance.

short-circuit test, the leakage of the primary and secondary windings is measured in series so that the effect is weakened.

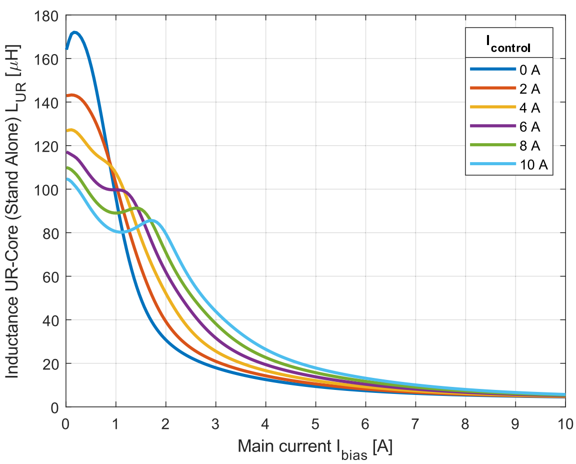

FIGURE 30. Inductance of the UR core.

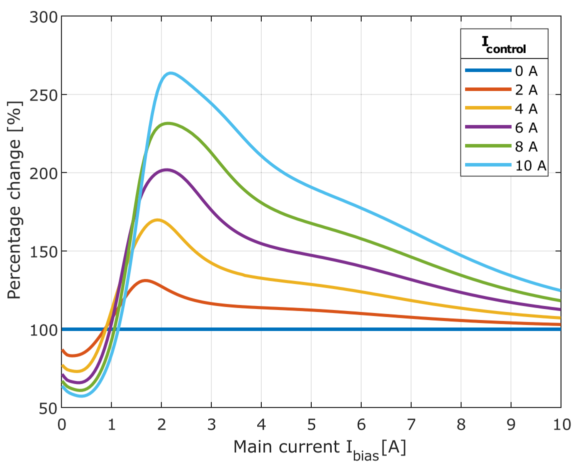

FIGURE 31. Percentage change of the inductance of the UR core.

If an air gap (Kapton foil) is introduced into the UR core, the magnetic resistance of the structure is increased, thereby reducing the impact of the premagnetization. However, changes of up to 60 % are still achieved in the saturation range.

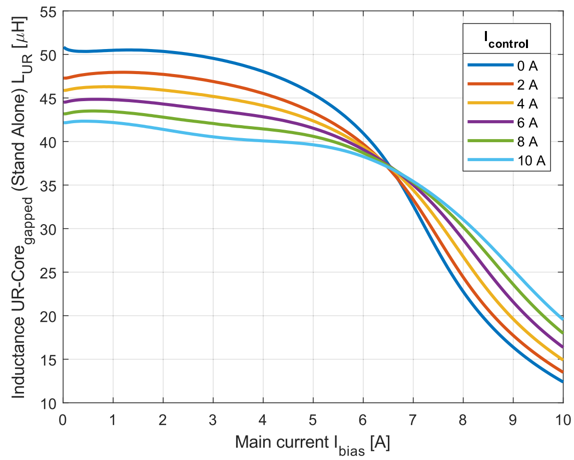

FIGURE 32. Inductance of the gapped UR core.

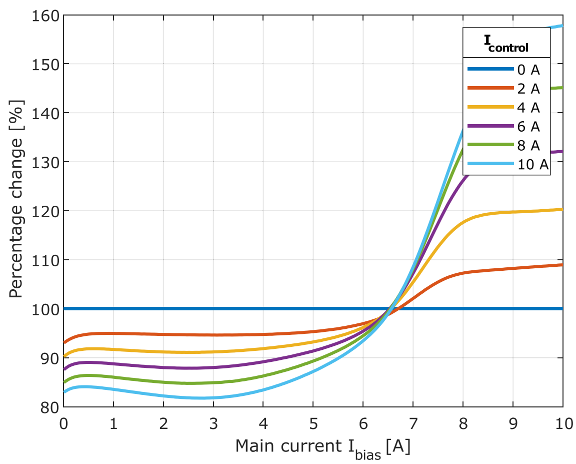

FIGURE 33. Percentage change of the inductance of the gapped UR core.

In summary, it can be stated that a controllable leakage inductance can be implemented without any major impact on the magnetizing inductance. The change in the inductance of the open-circuit measurement results only from the change in the leakage inductance, which is connected in series with the magnetizing inductance. Due to the influenceable permeability, which is reduced by an orthogonal auxiliary current, it could also be shown that the inductance for a certain operating point can not only be reduced but also significantly increased. The reason for this is that as the control current increases, the saturation knee is shifted towards higher field strengths, while the saturation flux density remains constant. It can also be seen that the greatest control effects can be realized with a core without an air gap, but in this case saturation occurs very quickly due to the main current of the primary or secondary winding. By introducing an air gap, the onset of saturation could, as expected, be shifted towards higher main currents, although the effect of controllability is reduced.

A transformer with controllable leakage inductance without significant effects on the magnetization inductance can be used in resonant topologies such as an LLC converter, for example. The additional degree of freedom gained could, for example, significantly reduce the required frequency range of the topology. Furthermore, a controllable leakage inductance can be used in a Dual Active Bridge (DAB) to either reduce the phase shift or to achieve soft switching again with a given phase shift, which significantly reduces the switching losses.

Further investigations are to be carried out. In particular, the use of mixed biasing in the UR cores could be of great interest because it could allow a wider range of adjustment of the leakage inductance. However, as this article is focused on orthogonal biasing, this consideration is beyond its scope.

VIII. COMPARISON OF THE DIFFERENT DESIGN APPROACHES

This section provides an overview of the variable inductors and transformers from the previous sections.

In addition, they are compared with each other in terms of their inductance variation. The specified values were determined considering ungapped implementations of the investigated magnetic components and under small variations of the main magnetic flux density, i.e. within the linear region of the equivalent magnetization curve.

TABLE 5. Comparison of the presented variable inductor approaches.

Core type	Figure	Inductance variation	
		Model	Experimental
Drilled EE core (EE 80/38/20)	4	425 %	172 %
Drilled URR core (URR 70/50/22)	4	96 %	626 %
Pot Core (P 148/112/10)	7	1005 %	636 %
Modified pot core (P 148/112/10)	9	1005 %	1032 %
UR core core (UR 64/40/20)	12	734 %	396 %
Modified UR core (UR 64/40/20)	12	734 %	2153 %

Table 5 summarizes the variable inductors. Where available, the results of the theoretical modeling and the experimental measured values are given. The comparison of the transformer design approaches is shown in the Table 6.

The variations in inductances presented in both tables account for the total change in reluctance, with the premagnetized state serving as the reference. This means that the reluctance value increases with a decreasing control current. This approach can be useful depending on the application. For instance, in a Dual Active Bridge (DAB) converter as shown in [23] and resonant converters in [24], the variation reflects increases in power or shifts in resonant frequency due to the control of the transformer parameters. For this reason, the following calculation method was used to indicate the range of variation:

$$\Delta L = \left| 1 - \frac{L(@I_{Aux} = 0A)}{L(@I_{Aux})} \right| \tag{7}$$

In other studies, particularly those involving controllable inductances, the non-premagnetized state is used as the reference as presented in [15], [25], [26], and [27]. As a result, variations in inductance are expressed as a percentage reduction, sometimes yielding negative values.

It has to be mentioned, that various factors impact the total variation in reluctance of magnetic devices when orthogonally biased, referring to the arrangement of the main and auxiliary windings. It was shown in Section IV that the air gap significantly impacts inductance variation, which is crucial for making accurate comparisons.

Additionally, the core geometry has been shown to cause discrepancies between the experimental and theoretical results, as it can be seen in Table 5. Theoretical models assume a purely orthogonal interaction between the main and control fluxes, but in practice, this interaction is not perfect (see Fig. 2). This can result in either larger variations in reluctance due to the presence of other flux interactions or smaller variations due to non-uniform control flux distribution within the core.

Comparing different implementations is challenging because the proportion between the main transversal area and the auxiliary winding area varies. For example, in the EE core implementation shown in Fig. 4, premagnetization affects only one-third of the core, while in the structure shown in Fig. 7, the entire core is magnetized. Furthermore, in some cases, the maximum control current density was not clearly defined. These observations highlight the need for standardized metrics to enable fair comparisons across different implementations.

Even a comparison between controllable magnetic devices and conventional ones has to be made within the context of a specific application. For example, the effective reduction in inductance volume for a DC/DC converter, presented in [26], due to premagnetization cannot be directly applied to other applications, such as Dual Active Bridge (DAB) converters in [23], where this feature led to a decrease in power density but improved efficiency and controllability. However, it should be noted that using active premagnetization requires additional control circuitry and transformer windings, which increases the complexity of the application.

Nonetheless, the presented work offers valuable insights and experimental findings that contribute to the development of improved core geometries for controllable transformers and inductors using orthogonal biasing. Although challenging, this technique offers unique advantages over traditional parallel biasing methods.

IX. DISCUSSION AND OUTLOOK

In this section, the results presented are critically examined and discussed. This gives rise to further research topics and approaches for the further development of the designs presented.

As already mentioned in Section VIII, the results presented are always related to the core material used, the core geometry used and the application. The selected approaches have to be considered in the context of the application and cannot simply be generalized.

The summary of the inductors in Table 5, also shown in Section VIII, shows clear deviations between the results of the theoretical modeling and the experimental measurement

TABLE 6. Comparison of the presented variable transformer approaches.

Core type	Figure	Transformer's parameter variation		
		Equivalent leakage inductance L_a	Equivalent magnetizing inductance L_b	Equivalent turns ratio N_e
Modified UR core (UR 64/40/20)	22	166 %	80 %	110 %
EE core (EE 55/28/21) & 2x UR Core (UR 37/26/18)	24	106 %	0 %	27 %

results. In this respect, a more detailed theoretical model is required that adequately depicts the processes of active premagnetization in the core material. This will provide a better understanding of the effects of this technology.

The modelling of active premagnetization is also closely linked to the issue of possible superposition effects. As explained in Sections II and V, pure orthogonal biasing does not occur in most core geometries. Depending on the core geometry, the effects of mixed or parallel biasing can be superimposed, especially with high modulation. However, the nature of this superposition, its onset and numerous other related effects have not yet been investigated.

The associated impact of the core geometry on the effect of active premagnetization has also only been investigated very rudimentarily.

The investigations and design approaches shown relate to the change in reluctance and thus the inductance value of the magnetic components. However, any associated impact on the core losses was not investigated. Since significant deformations of the hysteresis were determined and demonstrated in the investigations presented, it can be assumed that there is at least an impact on the hysteresis losses of the magnetic core. In addition, depending on the application, the auxiliary current could have either a positive or negative impact on the DC bias losses of the core material.

The investigations presented relate only to the actively premagnetized magnetic component. With regard to its use in a converter, however, the overall system should also be taken into account. It is therefore clear that an additional circuit is required to provide the auxiliary current. Furthermore, a control system for the active premagnetization has to be implemented. This additional effort has to be set in relation to the benefits of active premagnetization.

Other possible effects on the overall system should also be considered. It is possible, for example, that active premagnetization may result in increased filtering effort, which may partially or even completely offset the advantages gained in terms of volume, weight, efficiency or costs. This has to be considered in detail for each application.

X. CONCLUSION

Active premagnetization is a promising approach to making magnetic components controllable and thus gaining an additional degree of freedom in the design of the magnetic component or even the topology.

A distinction is made between parallel, mixed and orthogonal biasing. Orthogonal biasing is particularly interesting because feedback effects on the auxiliary control winding can be reduced very effectively. The effect of this premagnetization method is a shearing of the magnetization curve.

Orthogonal biasing often requires holes to be drilled in the magnetic core. This can be very difficult, especially with ferrite, because ferrite is a ceramic material that is very brittle. For other core materials, such as cut strip cores or laminated sheet metal cores, it is essential to check the feasibility in advance, espevially regarding changes of the magnetic properties. Another important factor is the air gap in the core. As shown in the article, this reduces the effect of active premagnetization, so that more auxiliary current is required to achieve the desired reduction in the inductance value.

Transversal core area compensation was proposed as a viable solution to improve the practical implementation of controllable magnetic devices under orthogonal biasing. However, core geometry modification can lead to significant changes in the main and control flux interactions, manifesting as a mixed or parallel bias pattern under certain conditions. Therefore, additional research is required to clearly establish the associated trade-offs. The implementation variable transformer using orthogonal biasing has been demonstrated. By increasing the control current, the effective number of turns is effectively reduced, leading to a decrease in both the equivalent series and parallel inductances. Notably, achieving significant changes in the effective turn ratio while maintaining a relatively high ratio between the parallel and series inductances requires substantial variations in the reluctance $\Re_v$. This desired variation has been achieved through the modification of the core structure by grinding the inner side of the limbs.

A transformer with adjustable leakage inductance was also presented. This can be significantly reduced by using active premagnetization, but can also be increased at some operating points. The magnetization inductance is hardly affected by the selected method, so that it remains virtually unchanged.

The investigations shown in this article are of particular interest for resonant converters and applications with Dual Active Bridge (DAB).

ACKNOWLEDGMENT

The authors would like to thank SUMIDA Components and Modules GmbH, Germany, and SMA Magnetics Sp. z o. o., Poland, for the manufacturing and customization of the cores used for the presented investigations. Responsibility of the content of this publication lies with the authors.

REFERENCES

[1] M. S. Perdigao, M. Menke, A. R. Seidel, R. A. Pinto, and J. M. Alonso, "A review on variable inductors and variable transformers: Applications to lighting drivers," Presented at the IEEE Ind. Appl. Soc. Annu. Meeting, Oct. 2014, doi: 10.1109/IAS.2014.6978431. [Online]. Available: https://ieeexplore.ieee.org/document/6978431

[2] M. S. Perdigao, J. M. Alonso, D. G. Vaquero, and E. S. Saraiva, ''Magnetically controlled electronic ballasts with isolated output: The variable transformer solution,'' *IEEE Trans. Ind. Electron.*, vol. 58, no. 9, pp. 4117–4129, Sep. 2011, doi: 10.1109/TIE.2010.2102315. [Online]. Available: https://ieeexplore.ieee.org/document/5675678

[3] G. Steiner, H. Zangl, P. Fulmek, and G. Brasseur, ''A tuning transformer for the automatic adjustment of resonant loop antennas in RFID systems,'' Presented at the IEEE Int. Conf. Ind. Technol., ICIT, Dec. 2004, doi: 10.1109/ICIT.2004.1490196. [Online]. Available: https://ieeexplore.ieee.org/document/1490196

[4] D. S. L. Dolan and P. W. Lehn, ''Finite element analysis of a virtual air gap variable transformer,'' Presented at the Can. Conf. Elect. Comput. Eng., 2008, doi: 10.1109/CCECE.2008.4564664. [Online]. Available: https://ieeexplore.ieee.org/document/4564664

[5] V. Majchrzak, G. Parent, J.-F. Brudny, V. Costan, and P. Guuinic, ''Coupling transformer with a virtual air gap for the protection of dynamic voltage restorers,'' Presented at the IEEE 40th Annu. Conf. Ind. Electron. Soc., Nov. 2014, doi: 10.1109/IECON.2014.7048541. [Online]. Available: https://ieeexplore.ieee.org/document/7048541

[6] V. Molcrette, J.-L. Kotny, J.-P. Swan, and J.-F. Brudny, ''Reduction of inrush current in single-phase transformer using virtual air gap technique,'' *IEEE Trans. Magn.*, vol. 34, no. 4, pp. 1192–1194, Jul. 1998. [Online]. Available: https://ieeexplore.ieee.org/document/706479

[7] S. P. Pesca, D. B. Cobaleda, C. Suarez, W. Martinez, and R. Diez, ''Analysis of wide voltage variation in LLC converters using variable transformers,'' Presented at the IEEE ANDESCON, Dec. 2022, doi: 10.1109/ANDESCON56260.2022.9989996. [Online]. Available: https://ieeexplore.ieee.org/document/9989996

[8] C. Suarez, D. B. Cobaleda, and W. Martinez, ''Analysis and validation of variable transformers,'' Presented at the IEEE 30th Int. Symp. Ind. Electron. (ISIE), Jun. 2021, doi: 10.1109/ISIE45552.2021.9576416. [Online]. Available: https://ieeexplore.ieee.org/document/9576416

[9] D. B. Cobaleda, F. Tian, C. Suarez, M. Vivert, and W. Martinez, ''Linear control compensator for a variable-transformer in wide-voltage power converters,'' Presented at IEEE 31st Int. Symp. Ind. Electron. (ISIE), Jun. 2022, doi: 10.1109/ISIE51582.2022.9831508. [Online]. Available: https://ieeexplore.ieee.org/document/9831508

[10] E. Haugs and F. Strand, ''Controllable transformer,'' U.S. Patent 2 467 989 C, Apr. 24, 2012. [Online]. Available: https://patents.google.com/patent/CA2467989C/en

[11] E. S. Tez, ''The parametric transformer,'' Doctoral thesis, Dept. Electron. Elect. Eng., Loughborough Univ., Loughborough, U.K., 2009. [Online]. Available: https://repository.lboro.ac.uk/articles/The_parametric_transformer/9520040

[12] J. Friebe, ''Permanentmagnetische vormagnetisierung von speicherdrosseln in stromrichtern,'' Doctoral thesis, Dept. of Elect. Eng., Univ. Kassel, Kassel, Germany, 2014. [Online]. Available: https://www.upress.uni-kassel.de/katalog/abstract.php?978-3-86219-820-7

[13] P. Zacharias, T. Kleeb, F. Fenske, J. Wende, and J. Pfeiffer, ''Controlled magnetic devices in power electronic applications,'' Presented at the 19th Eur. Conf. Power Electron. Appl., Sep. 2017, doi: 10.23919/EPE17ECCEEurope.2017.8099004. [Online]. Available: https://ieeexplore.ieee.org/document/8099004

[14] J. Pfeiffer, P. Küster, I. E. M. Schulz, J. Friebe, and P. Zacharias, ''Review of flux interaction of differently aligned magnetic fields in inductors and transformers,'' *IEEE Access*, vol. 9, pp. 2357–2381, 2021, doi: 10.1109/ACCESS.2020.3047156.

[15] J. Pfeiffer, ''Practical application of active premagnetization in transformerless DC/DC converters,'' Doctoral thesis, Dept. of Elect. Eng., Univ. Kassel, Kassel, Germany, 2023, doi: 10.17170/kobra-202211117096. [Online]. Available: https://kobra.uni-kassel.de/handle/123456789/14287

[16] J. Pfeiffer, C. Drexler, P. Küster, P. Zacharias, and M. Schmidhuber, ''Modeling the arrangement of drill holes for orthogonal biasing in controllable inductors for power electronic converters,'' Presented at 24th Eur. Conf. Power Electron. Appl., Sep. 2022. [Online]. Available: https://ieeexplore.ieee.org/document/9907309

[17] J. Pfeiffer, P. Küster, Y. Erenler, Z. H. S. Qashlan, and P. Zacharias, ''Impact of implementation of auxiliary bias-windings on controllable inductors for power electronic converters,'' Presented at the 22nd Eur. Conf. Power Electron. Appl., Sep. 2020, doi: 10.23919/EPE20ECCEEurope43536.2020.9215616. [Online]. Available: https://ieeexplore.ieee.org/document/9215616

[18] Z. H. Meiksin, ''Comparison of orthogonal-and parallel-flux variable inductors,'' *IEEE Trans. Ind. Appl.*, vols. IA–10, no. 3, pp. 417–423, May 1974, doi: 10.1109/TIA.1974.349171. [Online]. Available: https://ieeexplore.ieee.org/document/4157612

[19] H. Wouters, C. Suarez, and W. Martinez, ''Orthogonal biasing controllable inductor using a commercial hollow toroid core,'' Presented at the 11th Int. Conf. Power Electron. ECCE Asia, Jeju Island, South Korea, Aug. 2023, pp. 294–300, doi: 10.23919/ICPE2023-ECCEAsia54778.2023.10213978. [Online]. Available: https://ieeexplore.ieee.org/document/10213978

[20] C. S. Buitrago, D. B. Cobaleda, and W. Martinez, ''Magnetically controlled transformer with variable turns ratio and low series inductance: Analysis and implementation toward its application in SMPS,'' *IEEE Trans. Power Electron.*, vol. 38, no. 11, pp. 14360–14374, Nov. 2023, doi: 10.1109/TPEL.2023.3300583.

[21] C. Suarez and W. Martinez, ''Assessment of a DAB converter with a variable transformer by means of orthogonal premagnetization for wide voltage operation and enhanced efficiency at light-load conditions,'' Presented at the IEEE 8th Southern Power Electron. Conf. 17th Brazilian Power Electron. Conf. (SPEC/COBEP), Florianopolis, Brazil, Nov. 2023, pp. 1–7, doi: 10.1109/SPEC56436.2023.10407553. [Online]. Available: https://ieeexplore.ieee.org/document/10407553

[22] P. Zacharias, *Magnetic Components: Basics and Applications*. Wiesbaden, Germany: Springer Fachmedien Wiesbaden, 2022. [Online]. Available: https://link.springer.com/book/10.1007/978-3-658-37206-4

[23] S. Saeed, J. Garcia, and R. Georgious, ''Dual-active-bridge isolated DC–DC converter with variable inductor for wide load range operation,'' *IEEE Trans. Power Electron.*, vol. 36, no. 7, pp. 8028–8043, Jul. 2021, doi: 10.1109/TPEL.2020.3048928.

[24] Y. Wei, Q. Luo, X. Du, N. Altin, A. Nasiri, and J. M. Alonso, ''A dual half-bridge LLC resonant converter with magnetic control for battery charger application,'' *IEEE Trans. Power Electron.*, vol. 35, no. 2, pp. 2196–2207, Feb. 2020, doi: 10.1109/TPEL.2019.2922991.

[25] H. Hong, J. Zhang, M. Song, W. Gong, K. Cao, Y. Sun, J. Cui, D. Wang, Q. Li, B. Tian, Z. Wei, N. Zou, Z. Xiong, B. Shu, and Y. Xin, ''Magnetization study on a new type of orthogonally configured magnetic core structure and its potential application to superconducting controllable reactors,'' *IEEE Trans. Appl. Supercond.*, vol. 23, no. 3, Apr. 2013, Art. no. 5001004, doi: 10.1109/TASC.2013.2255943. [Online]. Available: https://ieeexplore.ieee.org/document/6491454

[26] D. Eichhorst, J. Pfeiffer, and P. Zacharias, ''Weight reduction of DC/DC converters using controllable inductors,'' Presented at the Int. Exhib. Conf. Power Electron., Intell. Motion, Renew. Energy Energy Manag., May 2019. [Online]. Available: https://ieeexplore.ieee.org/document/8767714

[27] G. Schierle, M. Meissner, and K. F. Hoffmann, ''Analysis and discussion of a concept for an adjustable inductance based on an impact of an orthogonal magnetic field,'' Presented at the 24th Eur. Conf. Power Electron. Appl., Sep. 2022. [Online]. Available: https://ieeexplore.ieee.org/document/9907399

JONAS PFEIFFER (Member, IEEE) received the Dipl.-Ing., M.Sc., and Dr.-Ing. degrees in electrical engineering from the University of Kassel, Germany. Since 2021, he has been a Development Engineer with the Advance Research and Development Department, SUMIDA Components and Modules GmbH, Obernzell, Germany. His research interests include controllable inductors and transformers, combined magnetic components, and volume and loss optimization of magnetic devices.

CAMILO SUAREZ BUITRAGO (Member, IEEE) was born in Tunja, Boyaca, Colombia. He received the B.Eng. degree in electronics engineering from the Universidad Nacional de Colombia, Bogota, Colombia, in 2011, the M.Sc. degree in electrical engineering from Universidade Estadual Paulista (UNESP), Ilha Solteira, São Paulo, Brazil, in 2017, and the Ph.D. degree in engineering technology from KU Lueven, Leuven, Belgium, in 2024.

PIERRE KÜSTER was born in Alsfeld, Hessen, Germany, in 1993. He received the B.Sc. and M.Sc. degrees in electrical energy systems from the University of Kassel, Germany, in 2017 and 2018, respectively, where he is currently pursuing the Ph.D. degree in electrical engineering. Since 2018, he has been a Research Assistant with the Department of Power Electronics, University of Kassel. His research interest includes the further development of magnetics for power electronics.

HANS WOUTERS (Graduate Student Member, IEEE) received the B.S. degree in electromechanical engineering from Hasselt University, in 2019, and the M.Sc. degree in electromechanical engineering from KU Leuven, in 2020, where he is currently pursuing the Ph.D. degree with the EnergyVille Power Electronics Research Group. Since 2023, he has receiving a fellowship from the Research Foundation Flanders (FWO). His research interests include electric vehicle charging, with a focus on efficient and compact magnetic design for bidirectional on-board chargers.

WILMAR MARTINEZ (Senior Member, IEEE) received the B.S. degree in electronics engineering and the M.Sc. degree in electrical engineering from the Universidad Nacional de Colombia, in 2011 and 2013, respectively, and the Ph.D. degree in electronic function and system engineering from Shimane University, Japan, in 2016. He was a Postdoctoral Researcher with the Toyota Technological Institute, Japan, in 2016, and Aalto University, Finland, in 2017. In 2018, he joined KU Leuven, Belgium, as an Assistant Professor with the Department of Electrical Engineering (ESAT), where he has been holding the position of an Associate Professor, since 2023. Additionally, he is also the Coordinator of the Research Line Power Electronics, EnergyVille, Belgium. His current research interests include a wide range of areas of power conversion for energy and transportation systems, battery charging infrastructure, and electric powertrain development through the multi-objective optimization of power converters, evaluation of iron losses of magnetic materials, and study of SiC and GaN switching devices.

JENS FRIEBE (Senior Member, IEEE) received the B.Sc., M.Sc., and Dr.-Ing. degrees in electrical engineering from the University of Kassel, Kassel, Germany. He was responsible for the research area of passive components in power electronics with the Institute for Drive Systems and Power Electronics, Leibniz University Hannover, Hanover, Germany, from 2018 to 2022. Before that, he was with SMA Solar Technology, Germany, in the field of PV-inverter topologies, wide-bandgap semiconductors, magnetic components, control strategies for high switching frequencies, and power electronics packaging, for more than 13 years. He is currently the Head of the Power Electronics Group, University of Kassel. He invented more than 30 granted patents in the field of power electronics.

MICHAEL SCHMIDHUBER received the degree in electrical engineering from the Technical University of Munich. After working as a freelancer, he is involved in several high-tech industry projects, and he finished the Ph.D. thesis. He is currently the Director of the Advanced Magnetics Research and Development Department, SUMIDA Components and Modules GmbH, Germany, dealing mostly with innovation, science, research, pilot, and pre-production studies, and governmental funded projects in the field of inductive components.